

# Starburst and old stellar population in the $z=3.8$ radiogalaxies 4C 41.17 and TN J2007–1316

B. Rocca-Volmerange<sup>1,4\*</sup>, G. Drouart<sup>2,1\*</sup>†, C. De Breuck<sup>2</sup>, J. Vernet<sup>2</sup>, N. Seymour<sup>3</sup>,  
D. Wylezalek<sup>2</sup>, M. Lehnert<sup>1</sup>, N. Nesvadba<sup>5</sup> and M. Fioc<sup>1</sup>

<sup>1</sup>*Institut d’Astrophysique de Paris, Université Pierre et Marie Curie/CNRS, 98bis Bd Arago, F-75014 Paris, France*

<sup>2</sup>*European Southern Observatory, Karl-Schwarzschild Strasse, 85748 Garching bei München, Germany*

<sup>3</sup>*AE (CSIRO Astronomy & Space Science), P.O. Box 76, Epping, NSW 1710, Australia*

<sup>4</sup>*Université Paris-SUD, 91405, Orsay Cedex, France*

<sup>5</sup>*Institut d’Astrophysique Spatiale, CNRS, Université Paris-Sud, 91405, Orsay, France*

Received 2012 August 10; accepted 2012 November 5

## ABSTRACT

Using the new evolutionary code PÉGASE.3, we made an evolutionary spectral synthesis of the optical-IR-submm spectral energy distribution of two distant ( $z = 3.8$ ) radio galaxies, 4C 41.17 and TN J2007–1316. These two radio galaxies were selected from the HeRGÉ (Herschel Radio Galaxies Evolution) Project in particular for their faint AGN contribution and because they show evidence of a large stellar contribution to their bolometric luminosity. PÉGASE.3 coherently models the reprocessing of the stellar luminosity to dust emission allowing us to build UV-to-IR-submm spectral energy distribution libraries which then can be used to fit spectral energy distributions in the observer’s frame. Our principal conclusion is that a single stellar population is insufficient to fit the spectral energy distributions of either radio galaxy. Our best fits are a sum of two evolving stellar populations – a recent starburst plus an old population – plus the thermal emission from an active galactic nucleus (which provides a good fit to the mid-IR emission). The two stellar components are: i) a massive ( $\approx 10^{11} M_{\odot}$ ) starburst  $\approx 30$  Myrs after formation, which is required simultaneously to fit the far-IR *Herschel* to submm data and the optical data ii) an older massive ( $\approx 10^{11-12} M_{\odot}$ ) early-type galaxy population,  $\approx 1.0$  Gyr old, which is required principally to fit the mid-IR *Spitzer*/IRAC data. A young population alone is insufficient because an evolved giant-star population produces a  $1 \mu\text{m}$  rest-frame peak which is observed in the IRAC photometry. This discovery confirms that much of the stellar populations in high redshift radio galaxies are formed by massive starbursts in the early universe. Gas-rich mergers and/or jet-cloud interactions are favored for triggering the intense star formation necessary to explain the properties of their spectral energy distributions. The discovery of similar characteristics in two distant radio galaxies suggests that multiple stellar populations, one old and one young, may be a generic feature of the luminous infrared radio galaxy population as a whole.

**Key words:** stars:formation-galaxies: evolution,active,stellar content -cosmology: miscellaneous-infrared: galaxies -radio continuum: galaxies

## 1 INTRODUCTION

Large scale cosmological simulations offer the prospect of constraining theories of galaxy formation and probing the appropriateness of cosmological parameters. However, hydrodynamical and N–body simulations meet various difficulties in fitting observations. The reasons for these difficulties is that there are many physical processes and timescales which are not well understood

such as: the appropriate initial conditions for the models, the detailed structure of dark matter halos, the timescale over which mass is accumulated into the halo and onto the galaxy, how stars form in detail, the relative role of major and minor mergers and their importance over cosmic time, the effect of the density of the galaxian environment and the impact of stellar and active galactic nuclei (AGN) feedback. Radio galaxies are known to be massive elliptical types which formed in the early Universe (van Breugel et al. 1998; Pentericci et al. 2001; Zirm et al. 2003; Lacy et al. 2011). The puzzling Hubble  $K - z$  diagram, which is bounded on the bright side principally by powerful radio

\* E-mail: rocca@iap.fr (BRV)

† ESO Doctoral Fellow

galaxies (Lilly and Longair 1984; De Breuck et al. 2002a), allowed us to identify in the comoving rest-frame the population of elliptical galaxies. This population is young but already massive ( $10^{12} M_{\odot}$ ) out to high  $z \approx 4$  redshifts (Rocca-Volmerange et al. 2004). On the other hand the mid-IR, far-IR and sub-millimeter emission from distant radio galaxies were interpreted as starbursts mainly initiated by major mergers (De Breuck et al. 2010; Ivison et al. 2008; Ivison et al. 2012; Engel et al. 2010; Seymour et al. 2010; Seymour et al. 2012). These dichotomous results: the old population from the Hubble  $K - z$  diagram and the young population from the need for high rates of star formation in radio galaxies imply that we are required to simultaneously follow the passive evolution of the galaxy as well as that of the on-going starburst to explain the overall spectral energy distribution (SED). To do this simultaneously requires a refined spectrophotometric model such as our new version of PÉGASE. The code PÉGASE.3 offers the possibility to interpret observations in the observer's frame by using UV-to-submm synthetic libraries built for a wide range of ages. The template SEDs take into account the local  $z=0$  templates corrected for evolution of the stellar population (e-correction) and redshift (k-correction). In the present paper we tackle a precise, heretofore still debated key issue—namely whether the most distant galaxies, including radio galaxies, are pure starbursts initiated by on-going mergers or are forming stars continuously on timescales longer than that generally appropriate for mergers. In radio galaxies, there is also the additional difficulty of the thermal emission from the AGN (perhaps a torus) and of the scattered light from the AGN which both contribute to the overall spectral energy distribution, especially in the mid-IR and UV respectively (Drouart et al. 2012). We chose two radio galaxies in particular, 4C 41.17 and TN J2007–1316, both at  $z=3.8$ , because of their small AGN contribution to the overall SED. We apply the following two selection criteria: (i) relatively faint scattered light contribution in the rest-frame UV as determined from polarimetric measurements. Polarimetric measurements are the only way to ensure that the continuum is mostly of stellar origin. Indeed those two galaxies are the only cases where a clear signature of photospheric absorption lines has been detected (Dey et al. 1997) (ii) faint contribution of the AGN in the rest-frame 8–12  $\mu\text{m}$  range of the SED. To fit the SED, one and two stellar components are successively tried from an automatic procedure which minimizes the  $\chi^2$ . We focus on the main properties (type, mass, age and star-formation history) of the two stellar populations. In § 2, we present the observations of the two radio galaxies for which we have built the continuous optical-IR-submm SEDs after correcting for instrumental effects (differing apertures, flux calibrations, etc.). PÉGASE.3 and the fitting method are described in § 3. § 4 presents the best fit results of SEDs in the observer's frame obtained using two evolved stellar populations plus a simple AGN model. Finally, we provide some thoughts on the implications of these results in § 5 and our conclusions in the last section. The adopted cosmological parameters are  $H_0 = 70 \text{ km.s}^{-1} \text{ Mpc}^{-1}$ ,  $\Omega_M = 0.3$ ,  $\Omega_{\Lambda} = 0.7$ .

## 2 OBSERVATIONS

The two radio galaxies 4C 41.17 ( $z \approx 3.80$ ) and TN J2007–1316 ( $z \approx 3.84$ ) are part of the sample of ultra-steep spectrum radio sources (USS;  $\alpha < -1.3$ ;  $S_{\nu} \propto \nu^{\alpha}$ ) designed specifically to increase the probability of discovering distant,  $z > 3$ , radio galaxies (De Breuck et al. 2000). The two targets were specifically selected because of their relatively low level of AGN activity in the

rest-frame UV/optical and their strong photospheric and dust signatures respectively seen in their optical continuum emission and in the cold dust-grain dominated far-IR emission. The *Spitzer* High Redshift Radio Galaxies (SHzRG) sample, which these two galaxies are also part of, were augmented with  $K$ -band photometry (Seymour et al. 2007; Seymour et al. 2008). Most of the complementary optical and submm photometry and data reduction procedures have been described previously (De Breuck et al. 2010). In addition, both galaxies have recently been observed by *Herschel* with the PACS (100 and 160  $\mu\text{m}$ ) and SPIRE (250, 350 and 500  $\mu\text{m}$ ) instruments, see also for 4C 41.17 (Wylezalek et al. 2012), and are part of the HeRGÉ (Herschel Radio Galaxy Evolution) Project (Seymour et al. 2012). Optical to submm spectral energy distributions, sampling the rest-frame photospheric (UV/optical/near-IR) stellar emission to emission from cold grains (far-IR) are carefully built paying specially attention to aperture effects, flux calibration, and flux transmission of the filters used for the observations and removing the contribution to the fluxes from strong emission lines. For the two galaxies the synchrotron emission is considered as negligible in the wavelength domain hereafter analyzed due to the steep radio spectra of the cores.

### 2.1 The radio galaxy 4C41.17

The radio galaxy 4C 41.17 ( $z = 3.800 \pm 0.003$ ) is the archetype of distant radio galaxies (Chambers et al. 1990). A detailed multi-frequency radio analysis with the VLA and MERLIN shows that the radio structure is associated with high resolution optical imaging *HST* data (Carilli et al. 1994; Miley et al. 1992). The galaxy is detected with a good signal-to-noise ratio and is spatially resolved at the 0.1'' *HST* resolution. Based on both the  $C_{III\lambda}$  to  $C_{IV}$  line ratio and the strength of the  $C_{IV}$  line, (Bicknell et al. 2000) suggested that there is an interaction of the high-powered jet with a dense cloud in the halo of 4C 41.17. Such an interaction through high speed shocks ( $\sim 1000 \text{ km/s}$ ), leads to strong compression of some of the gas, inducing star formation. The bright, spatially extended rest-frame UV continuum emission from this galaxy, aligned with the radio axis, is unpolarised ( $P_{2\sigma} < 2.4\%$ ) and shows tell-tale stellar absorption features indicative of on-going star formation (Dey et al. 1997). Two massive ( $M_{\text{dyn}} = 6 \times 10^{10} M_{\odot}$ ) components have been identified from CO(J=4–3) observations with the IRAM interferometer and interpreted as an evidence of mergers (De Breuck et al. 2005). However, the CO (J=1–0) emission line is not detected and the lower limits obtained are typical of molecular gas in starbursts (Papadopoulos et al. 2005). To complete the broad wavelength coverage of the SED of 4C 41.17, we use the total of the flux from 4C 41.17 within 6 arcsec field in the  $K_s$ -band, which is basically free of emission from strong optical emission lines (Graham et al. 1994). For the submillimeter emission we use the results from the JCMT (Dunlop et al. 1994) and IRAM (Chini et al. 1994).

The velocity and dispersion fields were mapped with the integral field spectrograph TIGER/CFHT (Adam et al. 1997) with a 0.61 arcsec spatial sampling. Radial velocities are essentially negative as the velocity field shows bow shocks with high velocity dispersions. Perpendicular to the main radio axis, a South-West extension of velocity =  $-600 \text{ km s}^{-1}$  and velocity dispersion =  $2000 \text{ km s}^{-1}$  is visible. Table 1 contains the photometry data we used to construct the SED of 4C 41.17. The upper limits and data not used by the fitting procedure are also provided for completeness and are also show in subsequent figures.

**Table 1.** Photometric data, in red on Fig. 3 and Fig. 4, of the radio galaxy 4C41.17 including new *Herschel*/SPIRE and PACS observations ( $\alpha(J2000) = 06^h50^m52.098^s$ ,  $\delta(J2000) = +41^\circ30'30.53''$ ). -tot- in column 4 means that galaxy photometry is totally measured within the instrument aperture. Complementary data, lower rows, in green on Fig. 3 and Fig. 4 are not used for fits, but are provided for completeness.

Filter( $\lambda_c \mu m$ )	FWMH	$F_\nu \pm \Delta_\nu (\mu Jy)$	Apert.	Refer.
<i>HST</i> _F702W(0.7)	0.15	$5.0 \pm 0.4$	$5.0''^2$	<i>a</i>
<i>KPN</i> <sub>I</sub> (0.9)	0.22	$4.5 \pm 2.6$	$15''$	<i>b</i>
<i>NIRC</i> <sub>I</sub> (1.25)	0.29	$5.6 \pm 1.1$	$2''$	<i>c</i>
<i>NIRC</i> <sub>Ks</sub> (2.15)	0.33	$13.6 \pm 2.8$	$8.0''$	<i>j</i>
IRAC1(3.6)	0.74	$23.4 \pm 2.4$	$12''$	<i>d</i>
IRAC2(4.5)	1.0	$27.5 \pm 2.8$	$12''$	<i>d</i>
IRAC3(5.8)	1.4	$35.6 \pm 3.7$	$12''$	<i>d</i>
IRAC4(8.0)	2.8	$36.5 \pm 3.5$	$12''$	<i>d</i>
PACS(170.)	80	$16.2 \pm 6.7 (+3)$	tot	<i>e</i>
SPIRE(250.)	100	$35.8 \pm 3.5 (+3)$	tot	<i>e</i>
SPIRE(350.)	150	$43.1 \pm 3.7 (+3)$	tot	<i>e</i>
SPIRE(500.)	200	$38.0 \pm 4.5 (+3)$	tot	<i>e</i>
UKT14(800.)	–	$17.4 \pm 3.1 (+3)$	tot	<i>h</i>
SCUBA(850.)	–	$12.1 \pm 0.9 (+3)$	tot	<i>g</i>
IRAM(1200.)	–	$4.4 \pm 0.4 (+3)$	tot	<i>f</i>
IRAM(1300.)	–	$2.5 \pm 0.4 (+3)$	tot	<i>i</i>
IRS(16)	–	upper limit	tot	<i>d</i>
MIPS(24)	6.6	$3.7 \pm 0.4 (+2)$	tot	<i>d</i>
PACS(70)	35	upper limit	tot	<i>e</i>

*a*:(Miley et al. 1992) *f*:(Greve et al. 2007)  
*b*:(Chambers et al. 1990) *g*:(Archibald et al. 2001)  
*c*:(van Breugel et al. 1998) *h*:(Dunlop et al. 1994)  
*d*:(De Breuck et al. 2010) *i*:(Chini et al. 1994)  
*e*:this paper, see also (Wylezalek et al. 2012)  
*j*:(Graham et al. 1994)

## 2.2 The radio galaxy TN J2007–1316, $z=3.84$

TN J2007–1316 (or WN J2007–1316) is also an ultra steep spectrum radio source selected from the 365 MHz TEXAS survey (Douglas et al. 1996) and the NVSS survey (Condon et al. 1998). It was also detected in the 352 MHz WISH survey and is part of the USS sample (De Breuck et al. 2002b). Spectropolarimetry of TN J2007–1316 obtained with FORS1 on the VLT on 3 nights from 2002 May 6 to 8 (Fig. 1). For these observations, the 300V grism was used with a  $1''$  wide slit oriented North-South and had a resolution of  $\sim 10 \text{ \AA}$  (FWHM). Conditions were photometric with seeing between 0.5–0.9 arcsecs. During each night, four equal-length exposures were taken using four different orientations of the half-wave plate ( $0^\circ$ ,  $45^\circ$ ,  $22.5^\circ$ ,  $67.5^\circ$ ). The total integration time was 27600s. The initial data reduction followed standard procedures in the NOAO IRAF package. Because the object is relatively faint in the single 35 or 40 minute exposures (each split into o- and e-rays), we needed to pay particular attention to extracting the same physical apertures in each of the individual spectra. We therefore first constructed the total 2-dimensional o- and e-ray spectra, and defined  $1 \times 2.4 \text{ arcsec}^2$  wide apertures from these spectra. We then used the aperture and trace of these spectra to extract the 12 o-ray and 12 e-ray spectra, using the same linear dispersion ( $2.645 \text{ \AA/pix}$ ) in order to calculate the polarization in equally-sized spectral bins. Finally, we combined these spectra using the median to construct the eight spectra needed to calculate the polarization vector. We followed the procedures of (Vernet et al. 2001) to calculate the polarization percentage and position angle. We checked the polarisation angle

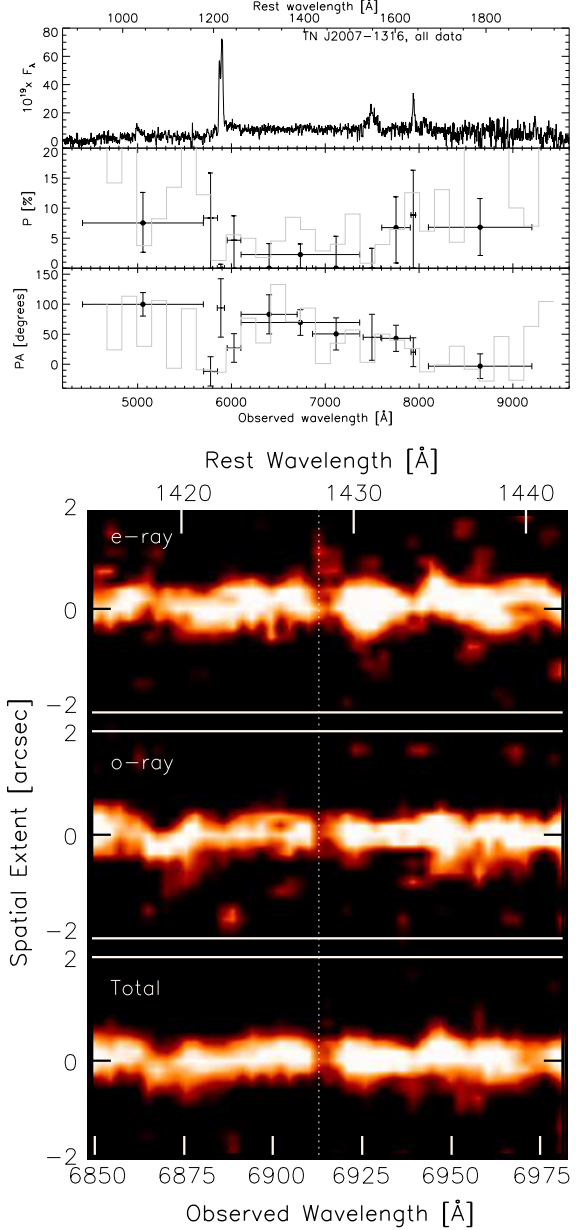


**Figure 1.** VLT spectropolarimetry of TN J2007–1316. the top panel is divided in three parts. The upper shows the total intensity spectrum, the middle plot is the percentage polarization, and the bottom panel the polarization angle, as function of observed wavelengths. Continuum bins are denoted by a dot. Vertical error bars denote  $1 \sigma$  uncertainties. The grey histograms show the data with a  $150 \text{ \AA}$  binning. The bottom panel is the 2D spectrogram, showing evidences of stellar signatures.

offset between the half-wave plate coordinate and sky coordinates against values obtained for the polarized standard stars Vela1 and Hiltner 652; our values are within  $<1^\circ$  from the published values, and the polarization percentage within 0.1 %. Table 2 provides the results and data source references.

## 3 THE EVOLUTIONARY CODE PÉGASE.3

The new version of PÉGASE.3 (Fioc, Rocca-Volmerange and Dwek, in preparation) predicts the evolution of the stellar

**Table 2.** Photometric data of the radio galaxy TN J2007–1316 (in red on Fig. 5),  $\alpha(J2000) = 20^h07^m53^s.23$ ,  $\delta(J2000) = -13^\circ16'43.6''$ . Complementary data (bottom lines) are not used for fits, only given for completeness. The continuum polarization percentage accurate to within 0.1 %.

Filter( $\lambda_c(\mu m)$ )	FWMH	$F_\nu \pm \Delta_\nu(\mu Jy)$	Apert.	Refer.
R(0.65)	0.06	$2.1 \pm 0.4$	$2.0''^2$	<i>a</i>
CFHT <sub>I</sub> (0.9)	0.22	$2.6 \pm 0.15$	$2.0''^2$	<i>a</i>
ISAAC <sub>H</sub> (1.65)	0.3	$9.6 \pm 1.0$	tot	<i>a</i>
UKIRT <sub>K</sub> (2.2)	0.3	$28.4 \pm 1.9$	$2.0''^2$	<i>d</i>
IRAC1(3.6)	0.74	$46.6 \pm 4.8$	tot	<i>a</i>
IRAC2(4.5)	1.0	$52.7 \pm 5.7$	tot	<i>a</i>
SPIRE(250.)	100.	$13.8 \pm 6.1 (+3)$	tot	<i>a</i>
SPIRE(350.)	150.	$16.5 \pm 6.4 (+3)$	tot	<i>a</i>
SPIRE(500.)	200.	$7.6 \pm 3.3 (+3)$	tot	<i>a</i>
SCUBA(850.)	–	$5.8 \pm 1.5(+3)$	tot	<i>b</i>
IRAC3(5.8)	1.4	upper limit	tot	<i>a</i>
IRAC4(8.0)	2.8	$135.1 \pm 16.9$	tot	<i>a</i>
IRS (16.0)	6.0	$378.0 \pm 113.$	tot	<i>c</i>
MIPS1 (24.)	6.6	$385.0 \pm 40.00$	tot	<i>c</i>
PACS(105)	40.	upper limit	tot	<i>a</i>
PACS(170)	80.	upper limit	tot	<i>a</i>

*a*: this paper

*b*: (Reuland et al. 2004)

*c*: (De Breuck et al. 2010)

*d*: (Bornancini et al. 2007)

continuum, of the the metal and dust content, the consequent attenuation and the re-emission of the UV/optical continuum by dust in a self-consistent manner. With this new version PÉGASE.3, updated from PÉGASE.2 ([www.iap.fr/pegase](http://www.iap.fr/pegase), (Fioc et al. 1997; Fioc and Rocca-Volmerange 1999b)), synthetic spectral energy distributions are continuously created from the far-UV to the sub-millimeter wavelengths at all ages ([www.iap.fr/pegase](http://www.iap.fr/pegase), (Fioc et al. 1997)). We built evolutionary scenarios which are consistent with the observed SEDs (and colors) of the full range of Hubble types at  $z=0$ . For convenience, we refer to these SEDs by their best fit of morphological Hubble types at  $z=0$ , with the understanding that they, by definition, represent the SEDs of galaxy representative their respective Hubble types in the local Universe. In PÉGASE.3, the chemical enrichment history is computed in an one-zone model, following the evolution of helium and most importantly, metals such as O, Ne, Mg, Si, S, Ca, C, Fe and N. We used the yields from (Marigo et al. 2001) for low- and intermediate-mass stars; those of (Woosley and Weaver 1995) and (Portinari et al. 1998) for high-mass stars; and model W7 of (Thielemann et al. 1986) for type Ia supernovae, see details in Fioc et al. in preparation. We assumed that dust formed in circumstellar environments (Dwek 1998): in the stellar winds of AGB and Wolf-Rayet stars, only carbon dust is produced if the C/O ratio is larger than 1 and only silicate dust otherwise; in supernovae, as CO is unlikely to form, both carbonaceous and silicate grains may form but with a lower efficiency than in other sources of dust. We compute the dust emission by distinguishing between two components: star-forming HII regions and the diffuse interstellar medium. Monte Carlo simulations of radiative transfer are computed including scattering by dust grains, for geometries typical of disks (exponential profiles for both stars and dust) and elliptical galaxies (King profiles). The path lengths of photons before escape, absorption, or scattering are obtained from the method of virtual interactions (Városi and Dwek 1999). The

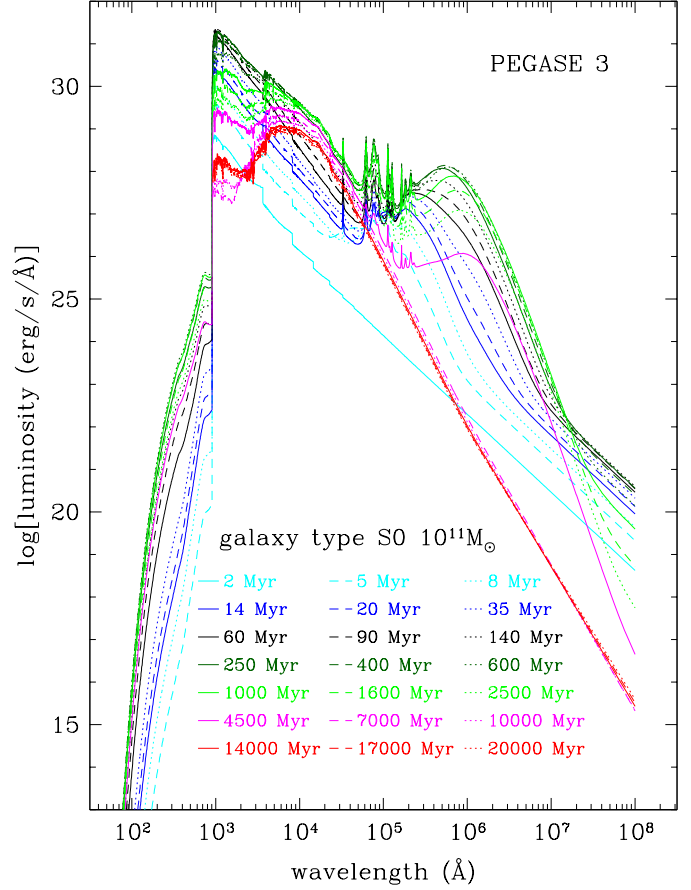


**Figure 2.** An example of SED templates for the  $10^{11} M_\odot$  S0-type galaxy at various stages of evolution as computed with PÉGASE.3. The  $1 \mu m$  peak of giant stars appears at ages  $\geq 1$  Gyr. Input parameters are: star formation rate  $= 2.10^{-3} \times$  current gas mass per Myr, infall time scale of 100 Myrs, galactic winds eject gas and dust at 5 Gyr, a Kroupa IMF, and spheroidal extinction model (see text for details).

attenuation is calculated for a grid of optical depths, albedos and asymmetry parameters, and the value at each wavelength is then interpolated on this grid. For each grain type and size, the probability distribution of temperatures is derived following the procedure detailed in (Guhathakurta and Draine 1989) i.e. with stochastic heating but assuming continuous cooling of grains.

To model a medium of higher gas density than the classical interstellar medium ISM we consider the optical depth depends simultaneously on the column density  $NH$  and the current metallicity (Guiderdoni and Rocca-Volmerange 1987). Following the formalism of (Dwek 1998) based on the respective fractions due to scattering  $\kappa_{sca}$  and to extinction  $\kappa_{abs}$ , the effective optical depth is:

$$\tau_{eff} = (\kappa_{abs} + \kappa_{sca}) \times K \cdot NH_{ISM} \cdot (Z_C + Z_{Si}) \cdot m_H \cdot 1.4$$

In case of denser absorbing/scattering media, the column density is multiplied by a  $K$  factor where  $NH_{ISM} = 6.8 \times 10^{21} \text{ atoms cm}^{-2}$  measured by mass unit of carbon and silicon in the interstellar medium of our Galaxy.

### 3.1 PÉGASE.3 libraries by types

Fig. 2 shows the example of the synthetic templates for a S0-type galaxy at various ages as computed by the code PÉGASE.3. Various synthetic libraries of SEDs evolving from ages of 0 to 20 Gyr are constructed to simulate the evolution of instantaneous starbursts and of galaxy types of Hubble sequence. Each star formation scenario is defined predominantly by a set of four parameters: star formation law, infall timescale, the epoch of galactic winds for early types and stellar initial mass function (see PÉGASE.2 readme on [www.iap.fr/pegase](http://www.iap.fr/pegase)). The parameter set of each type (Le Borgne and Rocca-Volmerange 2002; Fioc and Rocca-Volmerange 1999a) is chosen to predict  $z = 0$  SEDs and colors comparable by types to local observations (Fioc et al. 1997). The robustness of the adopted scenarios is checked on distant galaxies from the UV to the near-infrared  $K$ -band (Rocca-Volmerange et al. 2004). They are also tested on faint galaxy surveys analyzed by spectral types in the mid-IR (Rocca-Volmerange et al. 2007) and the UV-optical-nearIR domains (Fioc and Rocca-Volmerange 1999a). Moreover they are used for photometric redshift prediction out high redshift ( $z=4$ ) which shows substantial agreement with redshifts obtained spectroscopically (Le Borgne and Rocca-Volmerange 2002). Instantaneous starbursts are defined such that they form their stars over a period of 1 Myr. Then they passively evolve to the phase where their far-IR emission is dominated by the circumstellar emission of AGB stars and SN (the post-burst phase). The code computes by transfer this IR emission based on the efficiency at which the UV and optical photons are absorbed. Besides the SEDs by types, mass and age of the stellar populations are further outputs from the fitting procedure. Starburst libraries are computed for a variety of stellar initial mass functions (IMFs). For all scenarios, the IMF is taken from (Kroupa et al. 1993) after checking that other classical IMFs do not significantly change our predicted colours and template SEDs. Star formation is initiated at the redshift of formation that we denote as  $z_{for}$  taken as 10 when cosmic time slowly varies for redshift increases. While this would nominally imply an age of 13 Gyrs (adjusted to lower redshift for Irregulars, 9 Gyrs) for local  $z=0$  galaxies, this should not be taken as the average age of the stellar population as this is only when the star formation is initiated and not when the bulk of the stellar population forms (this depends on many factors of the models). Changing  $z_{for}$  from  $z=10$  to  $z=20$  or 30 will only vary typical ages of local templates by a small amount ( $\leq 0.4$  Gyrs) and thus resulting in only inconsequential variations in the SEDs.

### 3.2 Methodology

An automatic procedure which uses a  $\chi^2$  minimization searches for the best fit of observations. One or the sum of two spectral templates are from the set of synthetic libraries built for starburst plus a variety of SEDs fitting local Hubble type galaxies. For high redshift galaxies we work with template SEDs at redshift  $z$  in the observer's frame, by using the  $z=0$  template SEDs reproducing luminosities and colors of local galaxies. They are corrected for cosmological expansion (redshift  $k$ -correction) and for evolution (age  $e$ -correction) using the cosmic time- $z$  relation. For photometry through various filters, apparent magnitudes  $m_\lambda^i$  of galaxy type  $i$  through filter  $\lambda$  at age  $t$  and redshift  $z$  are computed by (Rocca-Volmerange and Guiderdoni 1988):

$$m_\lambda^i(t, z) = M_\lambda^i(t_0, 0) + (m - M)_{\text{bol}} + k_\lambda^i(z, t) + e_\lambda^i(z, t)$$

$M_\lambda^i(t_0, 0)$  is the local absolute magnitude by type  $i$ ,  $(m - M)_{\text{bol}}$  is the distance modulus and  $k_\lambda^i(z, t)$  and  $e_\lambda^i(z, t)$  are the expansion and evolution corrections, computed from PÉGASE.3 synthetic templates.

## 4 RESULTS OF THE SED FITTING

Because the two  $z=3.8$  radio-galaxies are selected for their small AGN contribution to the UV/optical portion of their spectral energy distributions as evidenced by their low level of polarization, simple models of the thermal emission from the AGN are sufficient for this analysis. The mid-IR SEDs provide an upper limit to the AGN component. We modeled the AGN emission of 4C 41.17 with a black-body at  $T = 600$  K and of TN J2007-1316 with the torus c model of (Pier and Krolik 1992) and (Krolik and Begelman 1988), see (Drouart et al. 2012) for details. A more robust statistical analysis of the contribution of the AGN in radio galaxies will be conducted for the whole of the HeRGÉ sample. For the two radio galaxies studied here, the range of plausible AGN thermal continuum models has only a minor impact on the results of our stellar SED modelling and will not be discussed further.

### 4.1 Single component model fits to the SEDs

Fig. 3left shows the best fits of the observed 4C 41.17 SED with one single burst of star formation with a duration of 1 Myr which is passively evolving for 25 Myr and also a single component spiral-like evolutionary scenario with an age of 1.6 Gyr. The starburst evolutionary scenario well fits the optical and far-IR (*Herschel*) data but fails to fit the region of the rest-frame  $0.4\text{--}2\mu\text{m}$  ( $K_s$  and IRAC/*Spitzer*) SED. The optical peak is due to stellar photospheric emission and the far-IR/sub-mm peak is due to a fraction of the  $N_{\text{Lyc}}$  photons absorbed by cold grains within environments of recent star formation. While the starburst episode is consistent with a substantial portion of the SED, (Seymour et al. 2012) for PKS 1138-262), having to let it evolve for  $\sim 25$  Myr suggests that the far-IR peak results from dust produced in and heated by supernovae and AGB stars while the optical (UV-redshifted) emission is due to the photospheres of recently formed mass stars. The AGN component, modeled as a blackbody with a temperature of 600 K, is compatible with data. The starburst mass, consistent with the best fit of the SED, is  $2.7 \times 10^{11} M_\odot$ . In case of instantaneous starburst, the average stellar metallicity  $\langle Z_* \rangle$  corresponds to the gas metallicity when stars were formed (null for a primitive cloud). For low values of  $\langle Z_* \rangle$  the far-IR emission is dominated by the self gas-enrichment of the starburst, measured by the parameter  $Z_{C+Si}$  which measures abundances of carbon and Silicon. The important point is that from the  $K_s$  and IRAC/*Spitzer* photometry, no matter what the exact starburst parameters are adopted, the mid-IR emission is not well fit. On the other hand, adopting a model with an older stellar population, such as an early-type spiral Sa scenario with an age of 1.6 Gyrs and having a stellar mass  $M_*$  of  $3.7 \times 10^{11} M_\odot$  while fitting the optical, NIR and *Spitzer*/IRAC data rather well, does not fit the far-IR emission (Fig. 3right). We note, because it is important evidence for the existence of an older population in both radio galaxies, that the SED of an older population shows a peak at around  $\sim 1\mu\text{m}$  which is clearly observed. However, despite obvious advantages to both models in fitting the SED, it is clear that neither single component model provides even an adequate fit to the overall SED.

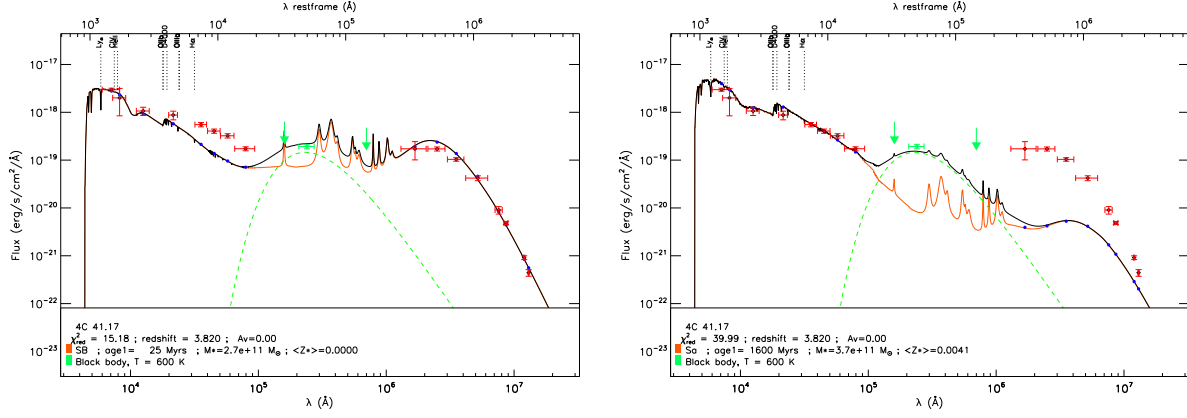


**Figure 3.** The multi-wavelength SED of 4C 41.17 (dots with red error bars) compared to the sum (black line) of two components: the AGN black body at  $T_{\text{eff}} = 600$  K (dashed green line) plus a stellar component: (left) a starburst at age 25 Myr; (right) a spiral Sa at age (time since  $z_{\text{for}}$ ) of 1.6 Gyr. The age, stellar metallicity, total stellar mass are derived from the best fitting model. Both of these single component models are missing a significant fraction of the total energy, either in the near-IR for the starburst or in the far-IR for the Sa-type galaxy evolutionary scenario. Vertical dotted lines mark the position of prominent emission lines. A second component is clearly needed to fit the SED. No intergalactic extinction ( $A_V = 0$ ) is taken into account in models.

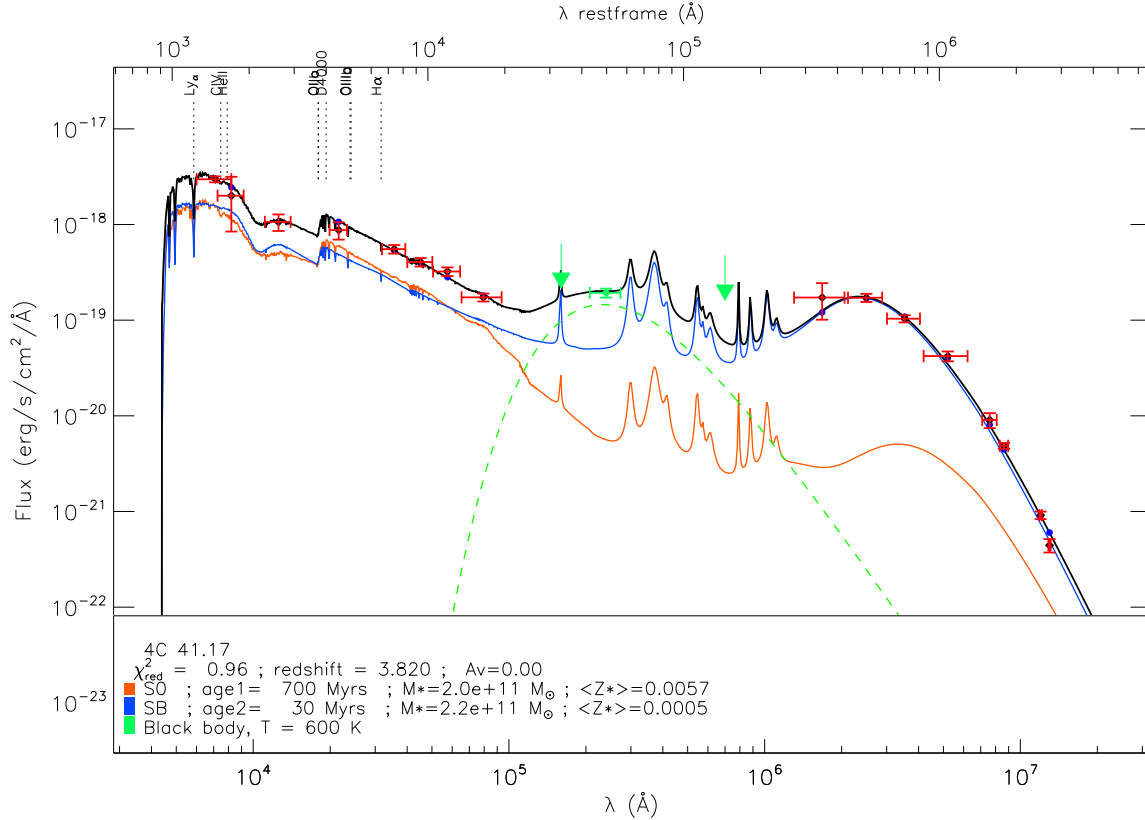


**Figure 4.** The SED of 4C 41.17 (dots with red error bars) including the new *Herschel* data is best fitted (reduced  $\chi^2 = 0.96$ ) by the sum (black line) of the S0-type population evolution scenario at age (time since  $z_{\text{for}}$ ) of 0.7 Gyr (orange line) and a starburst with an age of 30 Myrs after the initial 1 Myr duration burst (blue line) from a dense ( $10\times$  standard  $\text{NH}_{\text{ISM}}$ ) medium. A  $T_{\text{eff}} = 600$  K black body is used to model the thermal emission from the AGN (green dashed line). Observations not included in stellar fits are displayed in green. As can be seen, by excluding these data, our results are relatively insensitive to the exact model adopted for the thermal emission from the AGN. Vertical dotted lines mark the position of prominent emission lines. No intergalactic extinction ( $A_V = 0$ ) is taken into account in models.

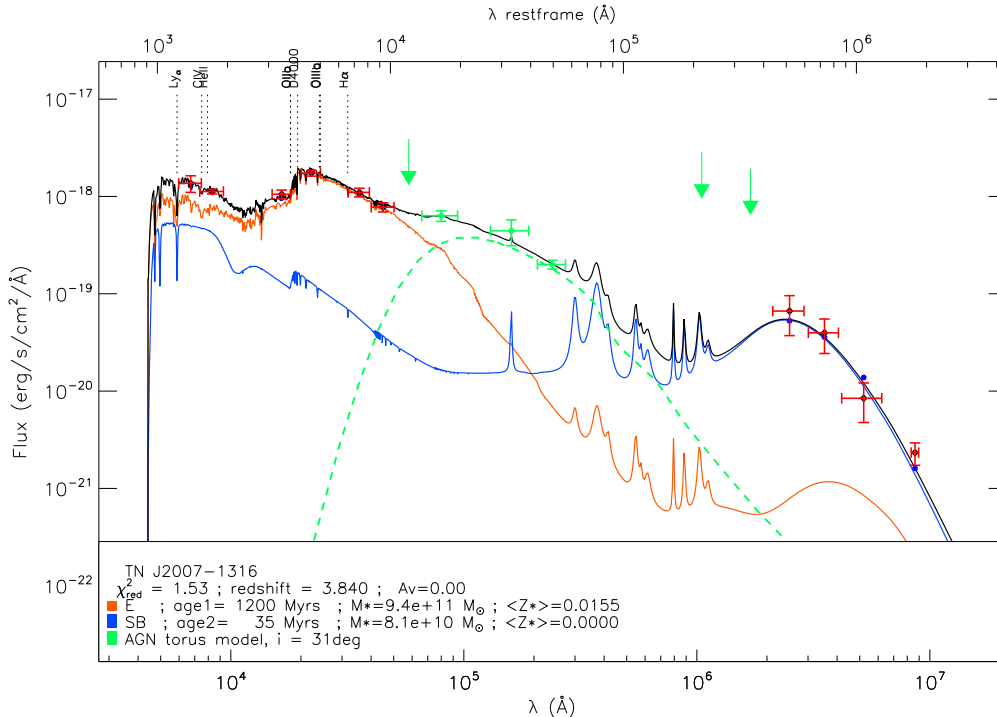


**Figure 5.** The multi-wavelength SED of TN J2007–1316 (dots with red error bars) including the most recent Herschel data is fitted (reduced  $\chi^2=1.53$ ) by the sum (black line) of an old (1.2 Gyr) elliptical galaxy (orange line) plus a starburst of 35 Myrs (blue line) from a dense medium of  $10\times$  standard  $N_{\text{HISM}}$  medium. The AGN model is the torus c model from Pier & Krolik (1992). Data points shown in green are not included in stellar fits. Vertical dotted lines mark the locations of prominent emission lines in the SED. No intergalactic extinction ( $A_V = 0$ ) is taken into account in models.

## 4.2 Two component model fits to the SEDs

Because the one component fits are inadequate but each individually have features which uniquely fit important regions of the overall SEDs, it seems logical to attempt two component fits which realize the advantages of each single component model. To this end, we fit two components, one representing a recent burst of star formation and the other, a passively evolving episode of past star formation (of course constrained by the age of the universe at  $z \sim 3.8$ ). The best fit scenario for the radio galaxy 4C 41.17 (Fig. 4) is a sum of the two stellar components: a vigorous starburst observed at age of 30 Myr from a cloud of stellar metallicity  $< Z_{\star} > = 5 \times 10^{-4}$  and mass  $M_{\star} = 2.2 \times 10^{11} M_{\odot}$  and a second population of a massive S0-type scenario with a short e-folding time (see Fig. 2) typical of early-types, observed at 0.7 Gyr after its initial formation epoch, with a stellar mass  $M_{\star} = 2.0 \times 10^{11} M_{\odot}$  and a metallicity  $< Z_{\star} > = 5.7 \times 10^{-3}$ . Results on stellar components are weakly sensitive to the adopted form of the AGN emission ( $T_{eff} = 600K$  blackbody model) in the portions of the SED which are likely dominated by the thermal IR emission from the AGN.

The results on the stellar components derived from the best fit for TN J2007–1316 (Fig. 5) are generally similar to those for 4C 41.17, namely there is the need for a young starburst and an older stellar population similar to that of a local massive galaxy evolved by a redshift of 3.8. Specifically, the fit requires a starburst of very low metallicity evolved for 35 Myrs with a total stellar mass of  $M_{\star} = 8.1 \times 10^{10} M_{\odot}$  and a second component consistent with that of an evolved massive early-type galaxy observed at age of 1.2 Gyr

(after  $z_{\text{for}}$ ) with the average stellar metallicity ( $\langle Z_* \rangle = 1.5 \times 10^{-2}$ ) and a significant stellar mass ( $M_* = 9.4 \times 10^{11} M_\odot$ ).

#### 4.2.1 A massive post-burst in distant radio galaxies

For the two  $z = 3.8$  radio galaxies, fitting simultaneously the optical ( $\approx 1500\text{\AA}$  rest-frame) and crucially the far-IR SED provided by the *Herschel*/submm data suggests that both galaxies are under-  
went a massive starburst several tens of Myr ago (a post-burst). The modeling of the far-IR emission depends on the metal-enrichment of Carbon and Silicon,  $Z_{C+Si}$ , while the observed UV-optical emission is dependent on the amount of absorbed photospheric emission intrinsic to the young stellar population. The main characteristics of the fitted young post-burst scenario are summarized in Table. 3. The best fit is a result of having to balance the far-IR and optical luminosities and spectral shapes, measured by the reduced  $\chi^2_{red}$  minimum. A younger age increases the number of Lyman continuum photons but decreases the metal-enrichment, favoring the direct photospheric emission relative to dust emission. Older ages have the opposite effect. Because of this dependence, the starburst mass and age are well constrained and unique. All other parameters of Table. 3 ( $Z_{C+Si}$  metallicity, supernovae number, high density value) are not free parameters, but derived from chemical evolution. We recall that the mean metallicity of stars  $< Z_{\star} >$ , as indicated in the legends, only traces the gas metallicity when stars were formed. In case of starbursts, this parameter is the initial gas metallicity and remains constant with age while gas metallicity evolves and is largely dominated at age of 30 Myrs by the intrinsic gas-enrichment due to the passive evolution of the starburst scenario.

**Table 3.** Characteristics of the young post-burst at  $z=3.8$ : age, stellar mass  $M_*$ , initial star formation rate, bolometric luminosity  $L_{bol}$ , dust/bolometric luminosity ratio, carbon+silicon  $Z_{C+Si}$ , mass fraction, column density factor  $K$  (NHI) =  $K \times \text{NHI}_{ISM}$ , and number of type-II SNe.

Post-burst	age Myrs	$M_*$ $10^{11} M_\odot$	$\text{SFR}_{init}$ $10^5 M_\odot \text{ yr}^{-1}$	$L_{bol}$ $10^{46} \text{ erg.s}^{-1}$	$L_{dust}/L_{bol}$	$Z_{C+Si}$	$K$ (NHI)	$n_{SNII}$ $10^7 \text{ Myr}^{-1}$
in 4C 41.17	30	2.2	2.6	8.0	0.96	0.026	10	7.1
in TN J2007–1316	35	0.8	0.1	0.3	0.97	0.025	10	0.3

**Table 4.** Characteristics of the old-star population at  $z = 3.8$ : age, stellar mass  $M_*$ , current star formation rate, bolometric luminosity, dust/bolometric luminosity ratio, Carbon+Silicate dust mass fractions, SNIa number, SNII number.

Early-type	age Gyrs	$M_*$ $10^{11} M_\odot$	$\text{SFR}_{current}$ $M_\odot \text{ yr}^{-1}$	$L_{bol}$ $10^{45} \text{ erg.s}^{-1}$	$L_{dust}/L_{bol}$	$Z_{C+Si}$	$n_{SNIa}$ $10^5 \text{ Myr}^{-1}$	$n_{SNII}$ $10^5 \text{ Myr}^{-1}$
4C41.17	0.7	2.0	243	8.2	0.522	0.026	0.8	19.2
TN J2007–1316	1.2	9.4	77	10.0	0.096	0.023	3.8	6.7

In the radio galaxy 4C 41.17 (Fig. 4 and Table. 3) the new *Herschel*/submm observations are well modelled by the cold grain emission of the highly massive and metal-enriched ( $Z_{C+Si}=0.026$ ) stellar environments. This post-burst population was triggered 30 Myrs earlier in a starburst with a duration of 1 Myr (instantaneous) with a star formation rate of  $2.6 \times 10^5 M_\odot \text{ yr}^{-1}$  (current stellar mass corrected for already died stars at age of 30 Myrs). The rapid evolution of most massive stars (a few  $10^7$  yrs) means that they have already evolved to SN and AGB stars when the post-burst is observed, enriching the interstellar medium. This implies that supernovae explosions ( $n_{SNII} = 7.1 \times 10^7$  by Myr) and AGB stars with circumstellar envelopes are dominant. A dense medium with the high column density (a factor  $K = 10 \times$  the column density measured in the Galaxy interstellar medium  $\text{NHI}_{ISM}$ ) is required by the far-IR data, implying  $10^{22-23} \text{ atoms cm}^{-2}$ . Such column densities have been found in radio galaxies (Mullaney et al. 2010). This post-burst in the far-IR dominates the total luminosity (96 %). In the radio galaxy TN J2007–1316 (Fig. 5 and Table. 3), the starburst age is 35 Myrs with a mass of  $8.1 \times 10^{10} M_\odot$  and an initial metallicity of zero, likely a primitive cloud. This suggests that most of the necessary metal enrichment to explain the far-IR emission ( $Z_{C+Si}=0.025$ ) was due to self-enrichment of the young stellar population.

#### 4.2.2 The importance of the $1 \mu\text{m}$ peak

Fig. 4 and Fig. 5 show the typical energy distribution of an old stellar population at wavelengths of the  $K$ -band and through *Spitzer*/IRAC filters (from the 4000 Å discontinuity to the typical  $1 \mu\text{m}$  peak in rest-frame). The evolution of early-type galaxies are characterized by a short ( $\approx 1$  Gyr) intense star formation episodes. This old population is seen in both targets perhaps suggesting it is a generic feature of radio galaxies. For both radio galaxies, this component has an age that is a significant fraction of a Hubble time at  $z=3.8$ . We recall that we have characterized the ages as the time from a formation redshift  $z_{for}$ , which for 4C 41.17 and TN J2007–1316 is roughly 0.7 Gyr and 1.2 Gyr respectively. However, acceptable fits allow for a range of age at least a factor of 2 around these nominal values. We also note that the bulk of the stars in this old population formed more recently than the values listed. This peak in the SED arising from evolved giant stars only evolves slowly and has been identified at all redshifts. This result supports our analysis of the Hubble  $K$ -band

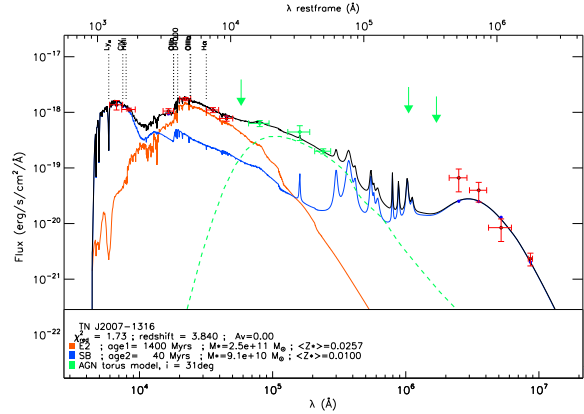
**Figure 6.** Best fit (reduced  $\chi^2=0.98$ ) of the multi-wavelength SED of TN J2007–1316 (dots with red error bars) with the sum (black line) of a 40 Myrs starburst (blue line) plus an early-type galaxy (1.4 Gyr) after an episode of galactic winds (orange line) ejecting gas and dust, they stop any further star formation. Masses and ages vary by  $\leq 50\%$  compared to results of Fig. 5.

diagram (Rocca-Volmerange et al. 2004), predicting already massive and old galaxies at  $z \geq 4$ . Table. 4 presents the characteristics of the evolved old component. Stellar masses are respectively  $2 \times 10^{11} M_\odot$  for 4C 41.17 and  $\approx 10^{12} M_\odot$  for TN J2007–1316. These masses are higher than that of the young starburst mass and perhaps suggest previous episodes of merging at earlier epochs. The contribution of the AGN to MIPS/*Spitzer* data, modeled by a simple black-body law at  $T_{eff} = 600 \text{ K}$  as shown on Fig. 4 (dashed green line), and by a more sophisticated torus c-model (adapted from (Pier and Krolic 1992) by (Drouart et al. 2012)) for the radio galaxy TN J2007–1316 (Fig. 5, dashed green line), does not change our conclusions: for these two radio galaxies, the AGN emission is not significant in the near-infrared domain at  $z = 3.8$ .

## 5 DISCUSSION

The SEDs of the radiogalaxies 4C 41.17 and TN J2007–1316 are revealed with two stellar, respectively young and old components and a simple AGN model. The spectral synthesis used to fit

the data is based on a variety of template libraries including instantaneous starbursts and evolutionary scenarios designed to fit the SEDs of local Hubble-type galaxies. Each scenario is characterized by a star formation time-scale:  $\sim 1$  Myr for the instantaneous starburst,  $\sim 1$  Gyr for ellipticals to  $\sim 10$  Gyrs for spirals (see (Rocca-Volmerange et al. 2004). In case of gas-dependent SF laws, star formation time-scales are regulated by the accretion and galaxy scale outflows of gas. One template library is built for each scenario. For starbursts, various standard IMFs are modeled in these template libraries. Because in evolutionary models as PÉGASE.3, IMFs are all normalized to  $1 M_{\odot}$  and is held fixed throughout the evolution, changing the IMF does have an effect on relative rate of metal-enrichment and dust fraction, but has only a minor effect on the best fit results of the SED. Although only weakly constrained, all of our best fits favor a (Kroupa et al. 1993) initial mass function. The most robust determinations from our fitting analysis are the relative ages and total stellar mass of each best fit scenario. For the two galaxies, our results suggest that shape of the SEDs is due to a vigorous recent starburst superimposed on a relatively evolved population whose formation was initiated at early epochs ( $z_{\text{for}} \geq 10$ ; but this is not when the bulk of the stellar population was formed, only when the star formation was initiated within the context of the scenarios used to model the SEDs). For the young starburst component, our results suggest an age of  $\sim 30$  Myr with a stellar mass of  $\approx 10^{11} M_{\odot}$ . The two peaks respectively seen in the optical and in the farIR/*Herschel* are the data which constrain this fitted component the most. This is because of the timescale for dust production in the postburst AGB and SN populations. Of much lower precision is the age of the older component which is mainly constrained by the peak at rest-frame  $1 \mu\text{m}$  due to slowly evolving giant stars. This slow evolution means that a wide variety of ages could in principle fit the data roughly equally well, but all best fit models suggest relatively old ages (100s of Myr). The best fits are that of an S0 galaxy with an age of 700 Myr for 4C 41.17 and an elliptical galaxy scenario with an age of 1200 Myrs for TNJ 2007–1316. Both are early-types with a  $\sim 1$  Gyr time-scale and masses of  $\approx 10^{11-12} M_{\odot}$ . To check the sensitivity of the 4C 41.17 results to ages of the models, we tested the relative variations in  $\chi^2$  for different models. We maintain an instantaneous starburst as first component. Replacing the second component by another starburst of 1 Myr duration induces a  $\chi^2$  variation of 10% and an age reduction of 80% with deeper balmer lines. Replacing the second component by an later-type (Sa) scenario with star formation scale of a few Gyrs induces a  $\chi^2$  variation of 5% and an age increase of 120%.

For TN J2007–1316, no other scenario, excepted ellipticals, is acceptable within a  $\chi^2$  variation of 400%. We also test (Fig. 6) a second component of an early-type model suffering galactic winds at early epochs (at age of 1 Gyr). The  $1 \mu\text{m}$  peak is then better fitted to IRAC data at age of 1.4 Gyr and summed with a younger (40 Gyrs) starburst. For the two populations, ages do not vary more than 50%.

In summary for these two powerful radio galaxies, the young post-burst and an evolved component of a short time-scale ( $\sim 1$  Gyr) are the best solutions. The timescale for both the increase in the metallicity with time and relative fraction of dust in the ISM which produced the far-IR emission are calculated in a self-consistent manner based on stellar yields and the production of dust by stars. The relatively poor time resolution in fitting the broad band continuum with stellar synthesis models for high redshift galaxies does not allow us to discuss anything but simple evolutionary models (not for example successive short bursts which would look more like continuous star formation in the models). Long star-formation

**Table 5.** Starburst/old population ratios

Radiogalaxy	ages	stellar mass	SNII number	factor K
4C41.17	30:700	2.2:2.0	71:1.9	10:1
TNJ 2007-1316	35:1200	8:94	30:6.7	10:1

time-scales results in two cumulated effects: increasing metal and dust fraction and simultaneously decreasing the photospheric emission of massive stars. Because of these effects, the parameter-range which simultaneously fits both the rest-frame optical and infrared portion of the SEDs is relatively narrow. That is why it is important to do this analysis on multiple sources, which if give consistent results, means that the general characteristics of the best fits are likely to be robust.

The general conclusions we can make are that the masses are likely in the range  $10^{10-11} M_{\odot}$  for recent starbursts and  $10^{11-12} M_{\odot}$  for the early-type evolutionary scenarios used to fit the data. Starbursts and evolved galaxies, have mass ratios of 1:1 to 1:10 typical of major mergers, so that any mass interchange will not significantly affect results. Moreover all mergers are gas-rich inducing an efficient star formation.

### 5.1 Star formation process in 4C41.17

What is triggering so intense star formation in distant radio galaxies? One of the most striking feature of these distant SEDs is the double peak of the starburst activity, respectively in the far-IR *Herschel* from dust and the optical, emitted from star photospheres. The instantaneous starburst model evolves to the age of  $\sim 30$  Myrs old likely dominated by supernovae and AGB stars. The huge stellar mass  $\approx 2.2 \cdot 10^{11} M_{\odot}$  corresponds to a rapid metal-enrichment from a no-primitive cloud ( $< Z_{*} \geq 5 \cdot 10^{-4}$ ). The emission is issued from a gas of high density, characterized by the factor  $K = 10$ , describing a ten time denser ISM than the classical interstellar medium. A model has been already proposed for 4C 41.17, a template of the so-called alignment effect (Chambers et al. 1990; Miley et al. 1992). Based on the jet-cloud interaction inducing star formation by shocks, suggested by many authors from 1980, it was revisited by (Bicknell et al. 2000) in the light of HST and radio emission line data (van Breugel et al. 1998; Dey et al. 1997). The authors conclude to a set of parameters: baryonic mass of  $\approx 8 \cdot 10^{10} M_{\odot}$ , a few Myrs star formation time-scale, a dynamic radio galaxy age of  $\approx 30$  Myrs and the high density of  $\approx 1-10 \text{ cm}^{-3}$ . All these values are compatible with our stellar population model, favoring the jet cloud interaction model for triggering star formation at high redshift. Another favorable argument for this scenario, at a much lower rate, is the star formation by jet-cloud interaction discovered in the core of NGC 1068 with the high angular resolution of NaCo/VLT (Exposito et al. 2011).

The dense medium measured by a column density factor  $K=10$  meaning  $10^{22-23} \text{ atoms cm}^{-2}$  only seen in the starburst component requires justifications. A better spatial resolution associated to a more refined 3D spectroscopy with the new generation of instruments (MUSE/VLT) will solve the location of star formation activity and the feedback measurement.

The coincidence of the short timescales of both starburst and jet-interaction could only be due to a similar causal origin. In that case, the post-burst we are seeing at works is only an episode of an active merger process. Many other arguments would favor massive gas-rich mergers at high redshifts. The discovery

of huge CO components (De Breuck et al. 2005; Engel et al. 2010; Ivison et al. 2012) already suggest evidences of major mergers in such powerful distant radio galaxies. Another convincing remark in favor of gas-rich mergers is that to form so huge stellar masses in short episodes requires large volumes of high gas-density. Table. 5 gives the characteristics of the intervening masses, with mass ratios typical of major mergers of young and evolved components of various metallicity, occasionally of primitive gas, implying several star generations through merger processes.

## 5.2 The old early-type stellar population

Local early-type galaxies are generally not luminous in the far-IR (Xilouris et al. 2004), which has been interpreted as the result of galaxy winds driven by the evolved populations (Mathews and Baker 1987). The other possible mechanism for driving winds is the mechanical and radiative energy from intense starbursts. For example, the local archetypal starburst galaxy M82, galactic winds were recently studied with *Herschel*/PACS (Contursi et al. 2012). The authors propose that cold clouds entrained in the galaxy disk outflow. At high redshifts, star formation activity is intense enough at the earliest epochs to induce intense winds which may also entrain the molecular and neutral atomic hydrogen driving it out of the galaxy. This assumption will possibly be statistically analyzed on the totality of the HeRGÉ sample.

The new important result is the emergence in the mid-IR (optical rest-frame) of an (already evolved) stellar component. Seen through the specific window (IRAC filters). The age and huge stellar mass of this old population is calibrated on the SEDs of two selected radio galaxies, in particular when galactic winds are imposed. At age of  $\sim 1$  Gyr, the evolved stellar population is giant stars building the well-known peak at  $1\mu\text{m}$  (rest-frame; Fig. 2). All these results favor the presence of highly massive early type galaxies initiated at early epochs  $z_{\text{for}} > 10$ , which must have grown very rapidly. Because the insufficient time resolution, the declining continuous star formation laws, as used in PÉGASE.3 and other codes could also be considered as a series of successive starbursts with intensities declining with time. From this point of view, which is also consistent with the data, the hierarchical assembly history of most massive ( $\sim 8 \times 10^{12} M_{\odot}$ ) haloes in a  $\sim 3 \text{ Gpc}^3$  volume as proposed in (Li et al. 2007) to form populations of  $z=6$  quasars would be compatible with our results.

## 5.3 The link with radio-quiet massive galaxies

The discovery of these  $z = 3.8$  old stellar component in powerful radio galaxies with a superposed starburst in a high density medium, warrants a comparison with radio-quiet early-type high- $z$  galaxies. These radio quiet galaxies have median stellar masses of  $\sim 4 \times 10^{11} M_{\odot}$  at  $z=2.0-2.7$  (Kriek et al. 2006). Their mass estimates are likely underestimated because observations were through the Gemini K<sub>s</sub> filter, missing the population of dominant rest-frame K-band emission redshifted in the *Spitzer* filters. However the comparison with powerful radio galaxies is justified because their respective masses are of the same order. Moreover deep and high-resolution images obtained with *HST*/NICMOS and /NIC2 and Keck (van Dokkum et al. 2008; Stockton et al. 2008) are associated to the presence of massive disks of old stars at high redshift of remarkably small sizes with a median effective radius,  $r_{\text{eff}}=0.9\text{kpc}$ . Cosmological surface brightness dimming has a strong impact on the perceived morphology of distant galaxies and likely explains

generally why disks are basically undetectable at  $z \geq 1.5$ . The decrement in surface brightness due to cosmological dimming is of  $\approx 7$  magnitudes at redshift 3.8. Only the central disk and spheroidal components are of sufficiently high surface brightness to be detectable even in deep images (Stockton et al. 2008).

If radio-load galaxies are a subpopulation of the massive radio-quiet galaxies which are undergoing an episode of vigorous star formation, it may well be that the powerful AGN illuminate the surrounding gas and dust in the disk over larger scales than would not otherwise be visible due to surface brightness dimming. Even the continuum emission would be affected due to scattering of the AGN continuum by dust. Moreover, in the population of radio-quiet massive galaxies, the stellar population does not have the massive young stellar component we have observed in IR-luminous powerful radio galaxies, and therefore would be less luminous in both the far-IR and in the optical perhaps below the threshold of the detectability. The massive evolved starburst in IR-luminous powerful radio galaxies contribute to the illumination of the disk over larger scales, sticking out of the surface brightness threshold. Observing extended emission preferentially in radio galaxies confirms the coexistence of the radio and starburst activity in the short star forming episode perhaps initiated by gas-rich mergers. Of course, the jet would also have an impact through its interaction with the surrounding gas, compressing and heating it. This shaping of the gas by the radio jet may also lead to stronger extended emission in both the emission lines and continuum.

More knowledge on kinematics and apparent morphology strongly modified by distance effects are also required for justifying the spheroidal structure of early-type galaxies. In case of radio galaxies, all these properties have to be associated to the presence of a supermassive black hole. Future studies will focus on the luminosity relationship between AGN and star formation activity of a larger sample of HeRGÉ galaxies.

## 6 CONCLUSIONS

From the PÉGASE.3 evolutionary spectral synthesis of two  $z = 3.8$  radio galaxies, the SED fitting on a large wavelength coverage (UV/optical to far-IR/submm), identifies two distinct stellar components. The originality and specificity of the analysis is to work in the observer's frame by using robust local templates, corrected at high  $z$  for the Universe expansion (k-corrected) and evolution due to distance (e-corrected), following scenario libraries by types of the code PÉGASE.3. At any time, synthetic templates are continuously computed with coherent UV/optical stellar emission and dust absorption reemitted in the far-IR. Instantaneous (1Myr) starbursts and a variety of scenarios of the Hubble sequence, varying with 1-10 Gyrs star formation time-scales, are considered for building template libraries. Best SED fits are derived in the observer's frame by a  $\chi^2$  algorithmic procedure on the sum of two stellar components plus a simple AGN model.

Main results are similar for the two galaxies at  $z = 3.8$ :

- one single component is unable to explain the complete spectral energy distribution, whatever types and ages.
- the sum of two stellar components give the best SED fits, following:
  - A 1 Myr starburst, observed at age of 30 Myr, forming a huge stellar mass  $\approx 10^{11} M_{\odot}$  in a dense ( $10\times$  standard ISM) medium, dominant in the far-IR *Herschel* to submillimetric and in the optical domains.
  - The discovery in the K-band to *Spitzer*/mid-IR domains

(1 $\mu$ m rest frame) of an already evolved ( $\approx 1$  Gyr at  $z = 4$ ) population.

- The evolved stellar component is compatible with an early-type galaxy (S0-Elliptical) initiated at early epochs ( $z_{\text{for}} \geq 10$ ), with possible galactic winds.

- The mass of the evolved component is huge of  $10^{11-12} M_{\odot}$  for the two galaxies at  $z \approx 4$ .

- The possibility of a gas-rich merger (joined to a possible jet-cloud interaction) is favored.

Over the longer term, we intend to include a more refined modeling of the AGN contribution to the overall SED in the PÉGASE.3 evolutionary synthesis models and to model the optical, *Herschel*/submm and *Spitzer* SED data of the HeRGÉ sample over its entire redshift range ( $1 \leq z \leq 5$ ).

## 7 ACKNOWLEDGMENTS

This work is based on observations taken at the European Southern Observatory with the Very Large Telescope, Paranal, Chile, with program ID 069.B-0078. It is also based in part on observations made with *Herschel*, a European Space Agency Cornerstone Mission with significant participation by NASA.

We finally thank the referee Dr. Alan Stockton for his helpful comments and suggestions which aided us in clarifying our arguments.

## REFERENCES

Adam, G., Rocca-Volmerange, B., Gerard, S., Ferruit, P., Bacon, R., 1997, *A&A*, 326, 501  
 Archibald, E., Dunlop, J., Hughes, D., Rawlings, S., Eales, S., Ivison, R. 2001, *MNRAS*, 323, 417  
 Bicknell, G. V., Sutherland, R. S., van Breugel, W. J. M., Dopita, M. A., Dey, A., Miley, G. K., 2000, *ApJ*, 540, 678  
 Bornancini, C. G.; De Breuck, C.; de Vries, W.; Croft, S.; van Breugel, W.; Röttgering, H.; Minniti, D., 2007, *MNRAS*, 378, 551  
 Carilli, C. L., Owen, F.N., Harris, D.E., 1994, *AJ*, 107, 480.  
 Chambers, K. C.; Miley, G.; van Breugel, W. J., 1990, *ApJ*, 363, 21  
 Chini, R.; Kruegel, E., 1994, *A&A*, 288, L33  
 Condon, J., et al., 1998, *AJ*, 115, 1693  
 Contursi, A., Poglitsch, A., Gracià-Carpio, J., Veilleux, S., and 10 co-authors, 2012, *arXiv:1210.3496*  
 De Breuck, C., van Breugel, W., Röttgering, H., Miley, G., 2000, *A&A*, 143, 303  
 De Breuck, C., van Breugel, W., Stanford, S. A., Röttgering, H., Miley, G., Stern, D., 2002, *AJ*, 123, 637  
 De Breuck, C., Tang, Y., de Bruyn, A. G., Röttgering, H., & van Breugel, W. 2002, *A&A*, 394, 59  
 De Breuck, C.; Downes, D.; Neri, R.; van Breugel, W.; Reuland, M.; Omont, A.; Ivison, R., 2005, *A&A*, 430, L1  
 De Breuck, C., Seymour, N., Stern, D., and 8 co-authors, 2010, *ApJ*, 725, 36  
 Dey, A., van Breugel, W., Vacca, W., Antonucci, R., 1997, *ApJ*, 490, 698  
 Douglas, J. N., Bash, F. N., Bozayan, F. A., Torrence, G. W., Wolfe, C. 1996, *AJ*, 111, 1945  
 Drouart, G., De Breuck, C., Vernet, J., Laing, R.A., Seymour, N., Stern, D., Haas, M., Pier, E.A., Rocca-Volmerange, B., 2012, *A&A*, 548, 45

Dunlop, J. S.; Hughes, D. H.; Rawlings, S., Eales, Stephen A., Ward, M. J. 1994, *Nature*, 370, 347  
 Dwek, E., 1998, *ApJ*, 501, 643  
 Engel, H.; Tacconi, L. J.; Davies, R. I.; Neri, R.; Smail, I.; Chapman, S. C.; Genzel, R., and 6 co-authors 2010, *ApJ*, 724, 233  
 Exposito, J.; Gratadour, D.; Clénet, Y.; Rouan, D., 2011, *A&A*, 533, 63  
 Fioc, M., Rocca-Volmerange, B., 1997, *A&A*, 326, 950  
 Fioc, M.; Rocca-Volmerange, B., 1999, *A&A*, 344, 393  
 Fioc, M., Rocca-Volmerange, B., 1999, *arXiv:astro-ph/9912179*  
 Graham, J. R., Matthews, K., Soifer, B. T., Nelson, J. E., Harrison, W., Jernigan, J. G., and 4 co-authors, 1994, *ApJ*, 420, L5  
 Greve, T. R., Stern, D., Ivison, R. J., De Breuck, C., Kovacs, A., Bertoldi, F., 2007, *MNRAS*, 382, 48  
 Guhathakurta, P., Draine, B. T., 1989, *ApJ*, 345, 230  
 Guiderdoni, B., Rocca-Volmerange, B., 1987, *A&A*, 186, 1  
 Ivison, R. J.; Greve, T. R.; Dunlop, J. S.; Peacock, J. A.; and 34 coauthors, 2008, *Cat.*, 83800199  
 Ivison, R., Smail, I., Amblard, A., Arumugam, V., De Breuck, C., and 12 coauthors, 2012, *arXiv:1206.4046*  
 Kriek, M., van Dokkum, P. G., Franx, M. and 11 co-authors, 2006, *ApJ*, 645, 44  
 Krolik, J. H.; Begelman, M. C., 1988, *ApJ*, 329, 702  
 Kroupa, P., Tout, C. A.; Gilmore, G., 1993, *MNRAS*, 262, 545  
 Lacy, M.; Petric, A. O.; Martı́nez-Sansigre, A.; Ridgway, S. E.; Sajina, A.; Urrutia, T.; Farrah, D. 2011, *AJ*, 142, 196  
 Le Borgne, D.; Rocca-Volmerange, B., 2002, *A&A*, 386, 446  
 Li, Y., Hernquist, L., Robertson, B., Cox, T., Hopkins, P., Springel, V. and 5 co-authors, 2007, *ApJ*, 665, 187  
 Lilly, S. J.; Longair, M. S. 1984, *MNRAS*, 211, 833  
 Marigo, P., 2001, *A&A*, 370, 194  
 Mathews, W. G.; Baker, J.C., 1971, *ApJ*, 170, 241  
 Miley, G. K., Chambers, K. C., van Breugel, W. J. M., Macchetto, F., 1992, *ApJ*, 401, 69  
 Mullaney, J. R.; Alexander, D. M.; Huynh, M.; Goulding, A. D.; Frayer, D., 2010, *MNRAS*, 401, 995  
 Papadopoulos, P., Greve, T. R., Ivison, R. J., De Breuck, C., 2005, *A&A*, 444, 813  
 Pentericci, L.; McCarthy, P. J.; Röttgering, H. J. A.; Miley, G. K.; van Breugel, W. J. M.; Fosbury, R., 2001, *ApJS*, 135, 63  
 Pier, E.A., Krolik, J.H., 1992, *ApJ*, 401, 99  
 Portinari, L., Chiosi, C., Bressan, A., 1998 *A&A*, 334, 505  
 Reuland, M.; Röttgering, H. J. A.; van Breugel, W.; De Breuck, C., 2004, *MNRAS*, 353, 377  
 Rocca-Volmerange, B.; Guiderdoni, B., 1988, *A&AS*, 75, 93  
 Rocca-Volmerange, B.; Le Borgne, D.; De Breuck, C.; Fioc, M.; Moy, E., 2004, *A&A*, 415, 931  
 Rocca-Volmerange, B.; de Lapparent, V.; Seymour, N.; Fioc, M., 2007, *A&A*, 475, 801  
 Seymour, N., Stern, D., De Breuck, C., Vernet, J., and 15 co-authors, 2007, *ApJS*, 171, 353  
 Seymour, N., Ogle, P., De Breuck, C., Fazio, G., Galametz, A., Haas, M., Lacy, M., Sajina, A., Stern, D., Willner, S.P., Vernet, J., 2008, *ApJ*, 681, L1  
 Seymour, N., Symeonidis, M., Page, M., HerMES consortium, the, 2010, *arXiv:1012.5085*  
 Seymour, N., Altieri, B., De Breuck, C., and 30 coauthors, 2012, *ApJ*, 755, 146  
 Stockton, A., McGrath, E., Canalizo, G., Iye, M., Maihara, T., 2008, *ApJ*, 672, 146  
 Thielemann, F.-K.; Nomoto, K.; Yokoi, K., 1986 *A&A*, 158, 17  
 van Breugel, W. J. M.; Stanford, S. A.; Spinrad, H.; Stern, D.;

- Graham, J. R. 1998, *ApJ*, 502, 614
- van Dokkum, P. G., Franx, M., Kriek, M., Holden, B., Illingworth, G. D.; Magee, D., Bouwens, R., Marchesini, D., Quadri, R., Rudnick, G., Taylor, E. N.; Toft, S., 2008, *ApJ*, 677, L5
- Városi, F.; Dwek, E., 1999, *ApJ*, 523, 265
- Vernet, J.; Fosbury, R. A. E.; Villar-Martín, M.; Cohen, M. H.; Cimatti, A.; di Serego Alighieri, S.; Goodrich, R. W., 2001, *A&A*, 366, 7
- Wylezalek, D.; Vernet, J.; De Breuck, C.; Stern, D.; Galametz, A.; Seymour, N.; Jarvis, M. and 12 co-authors, 2012, *MNRAS*, in press<sup>1</sup>
- Woosley, S. E.; Weaver, Thomas A., 1995, *ApJS*, 101, 181
- Xilouris, E. M., Madden, S. C., Galliano, F., Vigroux, L., Sauvage, M., 2004, *A&A*, 416, 41
- Zirm, A. W.; Dickinson, M.; Dey, A., 2003, *ApJ*, 585, 90